Efficiently Engineering Pore-Scale Processes: The Role of Force Dominance and Topology during Nonwetting Phase Trapping in Porous Media

Anna L. Herring[1], Linnéa Andersson[1], Steffen Schlüter[1,2], Adrian Sheppard[3], and Dorthe Wildenschild[1]

[1]*School of Chemical, Biological and Environmental Engineering, Oregon State University, Corvallis, OR 97331, USA*
[2]*Department of Soil Physics, Helmholtz-Centre for Environmental Research - UFZ, Halle, Germany*
[3]*Department of Applied Mathematics, Research School of Physics and Engineering, Australian National University, Canberra, ACT 0200, Australia*

Abstract

We investigate trapping of a nonwetting (NW) phase, air, within Bentheimer sandstone cores during drainage-imbibition flow experiments, as quantified on a three dimensional (3D) pore-scale basis via x-ray computed microtomography (x-ray CMT). The wetting (W) fluid in these experiments was deionized water doped with potassium iodide (1:6 by weight). We interpret these experiments based on the capillary-viscosity-gravity force dominance exhibited by the Bentheimer-air-brine system and compare to a wide range of previous drainage-imbibition experiments in different media and with different fluids. From this analysis, we conclude that viscous and capillary forces dominate in the Bentheimer-air-brine system as well as in the Bentheimer-supercritical CO_2-brine system. In addition, we further develop the relationship between initial (post-drainage) NW phase connectivity and residual (post-imbibition) trapped NW phase saturation, while also taking into account initial NW phase saturation and imbibition capillary number. We quantify NW phase connectivity via a topological measure as well as by a statistical percolation metric. These metrics are evaluated for their utility and appropriateness in quantifying NW phase connectivity within porous media. Here, we find that there is a linear relationship between initial NW phase connectivity (as quantified by the normalized Euler number, $\hat{\chi}$) and capillary trapping efficiency; for a given imbibition capillary number, capillary trapping efficiency (residual NW phase saturation normalized by initial NW phase saturation)

can decrease by up to 60% as initial NW phase connectivity increases from low connectivity ($\hat{\chi}$ ≈0) to very high connectivity ($\hat{\chi}$ ≈1). We propose that multiphase fluid-porous medium systems can be *efficiently* engineered to achieve a desired residual state (optimal NW phase saturation) by considering the dominant forces at play in the system along with the impacts of NW phase topology within the porous media, and we illustrate these concepts by considering supercritical CO_2 sequestration scenarios.

1.0 Introduction

During immiscible multiphase flow, drainage is the process of nonwetting (NW) fluid invading the pore space and displacing wetting (W) fluid, and imbibition is the process of W fluid invading the pore space and displacing NW fluid. Many engineered processes in the subsurface require fundamental understanding of drainage and imbibition processes and the resulting NW phase capillary trapping; for example, during oil recovery operations, remediation of non-aqueous phase liquid (NAPL) contaminants in the subsurface, and geologic sequestration of carbon dioxide (CO_2). In these examples, water is generally assumed to be the W phase; while oil, NAPL, or CO_2 are considered to be the NW phase. Although there are abundant exceptions to this assumption (e.g. intermediate-wet or oil-wet media), in this work we refer to water as the W phase for simplicity and consistency with previous work. In oil recovery and NAPL remediation processes the system already exists in the *initial* (post-drainage) state, i.e. both water and NW fluid (oil or NAPL) are already present in the system, and the bulk of previous research has focused on how to alter the imbibition (water flood) process to mobilize the maximum amount of trapped NW phase. Geologic CO_2 sequestration differs from oil recovery and NAPL remediation processes because both the drainage (i.e. CO_2 injection) and imbibition (i.e. water chase or groundwater flow) processes may be engineered, and the overall aim of the process is to trap, rather than mobilize, NW phase in the pore space of the geologic medium. From a CO_2 sequestration perspective, maximizing residual NW phase saturation is optimal; this is in comparison to oil recovery or remediation processes, in which minimal NW phase is the optimal residual state. Comparison between different studies and applications is complicated because fluid properties (e.g. density, viscosity, interfacial tension), medium properties (grain and pore size distributions, pore space connectivity, etc.), and flow properties (engineered injection or natural groundwater flow rates) vary widely depending on the application in question.

Recent focus on CO_2 sequestration as a global climate change mitigation strategy has prompted renewed study into the phenomena of capillary trapping in porous media (e.g. Juanes et al. [1], Al Mansoori et al.[2], Akbarabadi and Piri [3], Andrew et al. [4], among others). Capillary trapping of CO_2, wherein CO_2 is trapped by capillary forces in the pore bodies of a porous medium, is a relatively secure form of trapping, as compared to "structural" or "hydrodynamic" trapping, where the buoyant CO_2 is contained by an impermeable caprock; in addition, capillary trapping occurs on relatively short timescales, as compared to dissolution trapping or mineral trapping [5]. Thus, maximization of capillary trapping is important to ensure a safe and stable geologic carbon sequestration operation. Previous work has investigated NW phase capillary trapping over a wide range of fluid pairs, media types, and flow conditions for oil recovery and NAPL remediation applications. The results of these studies could greatly enhance fundamental knowledge that would benefit CO_2 sequestration studies if the results are appropriately compared and characterized. CO_2 is in a supercritical state at sequestration reservoir operations; relatively small variations in pressure, temperature, and salinity of the W phase have significant effects on the CO_2 density, CO_2 viscosity, and interfacial tension exhibited by the supercritical CO_2-brine system [6-8]. The variability of fluid properties complicates predictions of flow patterns and displacement mechanisms. Further, it has been shown that the initial (post-drainage) state of the reservoir has a substantial impact on the amount of residual capillary trapped NW phase present in the system after imbibition [9, 10]. However, experimental work with supercritical fluids is a non-trivial exercise, necessitating methods to approximate supercritical conditions with ambient experiments; Herring et al. [11] demonstrated that ambient condition micromodels were able to accurately predict the flow regime for a supercritical CO_2 drainage process in sandstone cores through application of a dimensional analysis.

We explore capillary trapping of NW phase from two perspectives. First, we investigate how consideration of the dominant forces at play via the *pore-scale force balance* in a system allows for comparison and better understanding of results from a wide range of experiments. The second study area results from the unique ability to engineer the drainage (CO_2 injection) process, and thus the initial (i.e. post-drainage) state. To this end, we use three dimensional (3D) metrics which can be used to describe NW fluid topology (connectivity) within porous media. In particular, we develop the relationship between initial NW fluid connectivity and the residual state of a system which was first investigated by Herring et al. [10], with new analysis of a high quality data set collected via x-ray computed microtomography (x-ray CMT) experiments performed at the Advanced Photon Source at Argonne National Laboratory. Finally, we provide physical interpretation of these relationships.

Consideration of pore scale forces and fluid topology allow drainage and imbibition processes to be efficiently engineered to provide favorable residual conditions. Geologic CO_2 sequestration scenarios are used as an example to illustrate these concepts.

2.0 Background

2.1 Pore scale forces

Considerable previous research has been conducted on the topic of residual (i.e. capillary trapped) NW saturation in porous media, with many different W and NW fluids, and in different media. To facilitate characterization of fluid flow over a range of properties, the experiments discussed in this work are characterized by the dimensionless ratios of capillary number (Ca) and Bond number (Bo).

Ca has been presented in several different forms, and has traditionally been defined from an oil extraction standpoint [12-14]. In general, Ca describes the balance between viscous forces and capillary forces with respect to the invading fluid (as opposed to the defending fluid). In this work, Ca is defined as:

$$\mathrm{Ca} = \frac{Viscous\ Force}{Capillary\ Force} = \frac{\mu_{INV} v_{INV}}{\sigma} = \frac{\mu_{INV}\frac{Q_{INV}}{A\cdot\eta}}{\sigma} \qquad \text{(eqn. 1)}$$

where μ_{INV} is the invading phase viscosity [mPa·s], v_{INV} is the invading phase Darcy velocity [m/s], and σ is the interfacial tension [mN/m] between the invading and defending fluid. The invading phase velocity is computed as the volumetric flow rate Q [m^3/s] divided by the cross-sectional area A [m^2] of the porous medium and the porosity η [-]. Note that while Ca is defined as a function of the invading fluid, and is thus dependent upon whether the system is undergoing imbibition (brine is the invading phase) or drainage (CO_2 is the invading phase).

Previous work has shown that under certain conditions, the Ca of the imbibition process determines the trapped NW saturation of the post-imbibition, residual state [12, 15, 16]. When a relationship between imbibition Ca and residual NW saturation is apparent, it is described by a constant residual saturation value for low imbibition Ca values with a sharp decrease in residual saturation as Ca of the imbibition process increases above the threshold or “critical” capillary number [14, 15]; this is shown in Figure 1 (modified from Cense and Berg [14]).

This relationship between Ca and NW saturation post-imbibition has been shown during NW desaturation experiments wherein the initial-state system (NW fluid is present in the medium) is water-flooded at increasing flow rates and the NW phase saturation in the core is measured as a function of Ca [14-17]; it is shown in sets of drainage-imbibition experiments conducted at different imbibition Ca [10, 16] and has also been supported by modeling results [18, 19]. However, Ca is not a complete descriptor of trapping in a porous medium, because the curves describing the dependence of residual saturation on Ca can shift due to changes in NW fluid properties [20] or medium properties [19]. Additionally, other experimental studies in different systems have found reduced or no dependence on Ca [21-23].

In a 3D system, the gravity force is considered via the Bond number (Bo); which here is defined as:

$$\text{Bo} = \frac{Gravity\ Force}{Capillary\ Force} = \frac{\Delta\rho \cdot g \cdot d^2}{\sigma} \qquad \text{(eqn. 2)}$$

where $\Delta\rho$ is the density difference between the two fluids [kg/m^3], g is the acceleration of gravity [m/s^2], and d is the representative length scale [m]. Here, in order to emphasize that forces are examined from a *pore-scale* perspective, as well as for ease of comparison with other studies, d is defined as the median grain diameter (or equivalent grain diameter for a micromodel); this is in agreement with Mohammadian et al. [24]. Note that while Ca is defined as a function of the invading fluid, and is thus dependent upon whether the system is undergoing imbibition or drainage, Bo is constant for a given fluid pair-porous medium system.

A combination of these two dimensionless numbers presents a description of the ratio of viscous to gravity forces:

$$\mathrm{Ca} \cdot \mathrm{Bo}^{-1} = \frac{Viscosity}{Capillarity}\frac{Capillarity}{Gravity} = \frac{Viscous\ Force}{Gravity\ Force} = \frac{\mu_{INV} v_{INV}}{\Delta\rho \cdot g \cdot d^2} \qquad \text{(eqn. 3)}$$

Following Polak et. al., [25] we will use a combination of the dimensionless numbers Ca and Bo to determine which forces are dominant during the imbibition process, on a pore-scale basis, in a 3D porous medium system. Figure 2 shows the location of a number of existing 3D multiphase flow studies overlaid onto the pore scale force balance diagram. As suggested by Polak et al. [25], we suggest that the relative location of a system within the pore-scale force balance illustrates which force(s) has the greatest impact on flow processes. In their study, Polak and colleagues demonstrated the interplay of all three forces (capillary, viscous, and gravity) resulting in a figure very similar to that shown in Figure 2; however, we have modified their original formulation via reformulation of the representative length scale *d* in Bo in order to more easily accommodate comparison of a wider range of experimental studies and to emphasize that we examine these systems on a pore-scale basis.

We note here that the Ca values presented in this work are derived from the traditional macroscopic formulation, in contrast with recent works which define Ca from a pore-scale perspective wherein properties of individual NW phase clusters are considered and incorporated into the Ca formulation [26, 27]. The pore-scale formulations [26, 27] more accurately describe the physics of mobilization of NW fluid on a pore-scale basis, but also require highly detailed and complete pore-scale descriptions of NW phase to adequately calculate Ca values. In our non-dimensional analysis, we utilize the traditional Ca as defined in equation 1 in order to facilitate inclusion of several previous studies for which detailed measures of individual NW fluid clusters are unavailable. Also note that media are assumed to be strongly wetting systems, as contact angle is not incorporated into the dimensionless numbers presented in equations 1-3. Finally, medium topology and morphology (coordination number, pore-throat aspect ratio) and other media features (e.g. porosity, consolidated vs. unconsolidated) which may also be important to multiphase fluid flow are not well-represented by this model; nor is the defending fluid viscosity. As a consequence of these limitations, this analysis should be considered to be an "order of magnitude" approximation.

The studies presented in Figure 2 lie within several general areas of force dominance. For studies with systems which lie in the upper right corner of the figure, both capillary and viscous forces are important; in this regime there is a transition between whether capillary and viscous forces dominate, and trends of residual saturation with Ca are evident; e.g. Chatzis et al. [16] found that residual saturation and NW blob morphology after imbibition was a function of Ca. However, in this area of the figure, gravity forces play a minor role, explaining the findings of Mayer and Miller [28] and Gittins et al. [29] which state that the bead/grain size (equivalent to *d*, a gravity force parameter) has no effect on the amount residual NW saturation. For experimental systems closer to the bottom left of the figure, gravity forces impact the experiments, e.g. the experiments of Morrow et al. [15] range from the capillary-viscosity dominated regime to the gravity dominated regime, and the results of that study demonstrate a significant dependence on both Ca and Bo. Moving down Figure 2 (further away from the capillary dominated regime and into gravity dominated space), the experiments of Mayer and Miller [21] showed that blob morphology exhibited a strong dependence on Bo, and only a very weak dependence on Ca. More recently, Harper et al. [22] found no correlation of residual NW saturation with Ca, but rather that Bo and defending phase viscosity were the most significant parameters. Similarly, Geistlinger et al. [23] found no correlation of residual saturation with Ca, and rather that trapped

NW phase is dependent on pore size distribution (again, a parameter which indicates gravity dependence).

This non-dimensional analysis explains the differences in findings of experimental studies with a large range of porous media, flow conditions, and fluid pairs; and resolves some of the seeming contradictions that have been observed by experimentalists. The location in the force dominance plot of the brine-air-Bentheimer sandstone experiments of this study are shown with the approximate location of supercritical CO_2 sequestration scenarios, given the range of supercritical CO_2 fluid properties attainable and assuming similar media to Bentheimer sandstone (Figure 2). In light of the above discussion, we expect capillary and viscous forces to dominate both the brine-air-Bentheimer ambient condition experimental system as well as a geologic supercritical CO_2 sequestration scenario.

2.2 Initial State Topology

Following Herring et al. [10], we refer to a system uniformly saturated with W fluid to be in the *original* state; a post-drainage system (i.e. NW is introduced to the system) as being in the *initial* state; and a post-imbibition system as the *residual* state. The well-documented capillary pressure hysteresis present in multiphase systems (e.g. Morrow, 1970 [30]) dictates that the residual state (and thus, trapped NW saturation) is dependent on the initial state. The relationship between initial and residual NW saturation (S_I and S_R, respectively) in porous media has been investigated and described empirically by the so-called Land's model; it has been established that as initial NW saturation increases, residual NW saturation increases towards a plateau-like maximum [2, 31]. An alternate means to visualize this relationship is to examine the "trapping efficiency" (i.e. S_R/S_I) as a function of initial NW saturation: S_R/S_I is highest at relatively low S_I values, and decreases as S_I continues to increase [3]. While these empirical relationships are well characterized for a variety of porous media systems, the underlying physical mechanisms for this behavior remain relatively poorly understood. As originally suggested by Wardlaw and Yu [32], and further examined by Herring et. al. [10], we propose that the reason for the plateau in the Land's model description of trapping and the associated decrease in trapping efficiency at high S_I values is due to high connectivity of the NW phase at high NW saturation: as the NW fluid becomes highly interconnected via increasing numbers of pore throats, the pathways available for mobilization dramatically increase.

We have previously investigated this phenomenon by examining trapping efficiency as a function of initial NW phase topology, specifically, as quantified by the initial normalized NW Euler number ($\hat{\chi}$) [10]. Herein, we further develop and compare this approach to another quantitative descriptor of connectivity, the gamma function (Γ), which is a statistical percolation metric described by Renard and Allard [33].

2.2.1 Topological Invariants

Topological invariants are properties of objects which are not changed by continuous deformations such as stretching, bending, and twisting; they are only changed when parts of an object are discontinuously deformed (i.e. "torn" or "glued together"). Topological invariants describe an object's connectivity; in comparison to an object's geometry, which describes its shape. The Euler number (χ) is a topological invariant defined as the alternating sum of the first three Betti numbers (β_0, β_1, β_2):

$$\chi = \beta_0 - \beta_1 + \beta_2 \qquad \text{(eqn. 5)}$$

where β_0 is the number of individual objects present, β_1 is the number of redundant loops or handles present (e.g. the handle on a coffee mug or the loop of a doughnut), and β_2 is the number of holes or hollows within the object(s) present. Previous studies have utilized Euler values to characterize connectivity of sintered copper porous cores [34] and bone tissue [35]. Applied to a fluid phase within a porous medium, β_0 can be thought of as the number of distinct, individual fluid clusters; β_1 is the number of redundant connections via pore throats within the clusters; and β_2 is the number of bubbles of a different fluid or solid particles suspended in the fluid. For this work, we investigate the topology of a less-dense NW fluid (air), which implies that β_2 will be zero (i.e. no "floating" water droplets or rock grains in the air phase). Thus β_2=0 for conversion between Euler number and Betti numbers; this is in agreement with analysis by Vogel [36]. A topological description of the connectivity of a fluid phase in a porous medium is fairly intuitive; during a drainage process, for example, as fluid clusters coalesce and grow together, the number of individual objects (β_0) decreases; and as more and smaller pore throats are invaded, the number of redundant connections within the fluid clusters (β_1) increases. This leads to an overall decrease in Euler number; therefore, as Euler number becomes more and more negative, the NW phase fluid is becoming better connected. At some critical value of NW saturation, the NW phase will be connected across the domain; the transition from dominantly disconnected ($\chi > 0$) to dominantly connected ($\chi < 0$) is related to the percolation threshold for a given phase [36, 37] and the saturation at which the Euler number is exactly zero is an estimate of the saturation percolation threshold for NW phase flow.

The Euler number is an *extensive* property of a system in that the overall Euler number for a domain is the sum of the values of all subdomains within it. Therefore the Euler number depends on the scale over which it is measured; the Betti numbers are also scale-dependent. Values of the Euler number or Betti numbers calculated on one section of an object are *local* (rather than *global*) values, and are therefore not representative of the total overall object, nor are they necessarily representative of other same-sized subsections of the object due to statistical variation or small-scale heterogeneities. However, appropriate normalization of the Euler or Betti values leads to a more representative metric. Herring et al. [10] calculated Euler numbers for the entire pore space (i.e. Euler numbers for systems at 100% NW phase saturation), and normalized the Euler number for the system at a given saturation by the Euler number at 100% NW phase saturation:

$$\hat{\chi}_{NW} = \chi_{NW}/\chi_{100\%NW} \qquad \text{(eqn. 6)}$$

This normalization results in a connectivity metric with a maximum value (most connected) of 1.0, where negative values indicate disconnectedness. A representative elementary volume (REV) analysis (see supplementary materials, available online) demonstrates that $\hat{\chi}_{NW}$ can be used as a representative measure of NW phase connectivity for a given sample. However, values of $\hat{\chi}_{NW}$ are highly dependent on the value of $\chi_{100\%NW}$, so accurate measurement of this parameter is essential.

2.2.2 Statistical Percolation Metrics

The term "percolation" refers to the transition from individual, disconnected clusters to one large cluster which spans the length of the porous domain; e.g. once a single NW phase pathway is established all the way through a porous medium, the NW fluid can be said to percolate through the media. Γ is a probability-based percolation metric described by Renard and Allard [33] and is defined here as a function of permeable phase saturation, *p*. In the context of NW phase fluid transport, we define the permeable phase *p* to be NW fluid: Γ(NW) is the ratio of the sum of squares of all individual NW phase cluster volumes to the square of the total NW phase volume present in the domain. From an image analysis perspective, Γ(NW) can be approximated by calculating the ratio of pairs of individual NW voxels that are connected to all the possible pairs of NW voxels, and can be computed directly from the cluster size distribution:

$$\Gamma(\mathrm{NW}) = \frac{1}{n_{NW}^2}\sum_{i=1}^{N(X_{NW})} n_i^2 \qquad \text{(eqn. 7)}$$

where n_{NW} is the total number of NW phase voxels in the set X_{NW}, $N(X_{NW})$ is the number of distinct clusters in the set X_{NW}, and n_i is the number of NW voxels in cluster i.

As Γ(NW) approaches 1.0, the fraction of the fluid that lies in a single cluster increases. In contrast to the *local* Euler values described above, this metric is *global*: whereas Euler number values can be measured on individual objects within the domain and subsequently summed to find the overall Euler number value for the entire domain, Γ(NW) must be computed over the entire domain of the system by necessity. By value of being a probability metric, Γ(NW) can be assumed to be representative of a given sample without further manipulation or normalization (again assuming a representative elementary volume has been achieved, see the supplemental materials (available online) for REV analysis of Γ(NW)). Also note that the definition of Γ inherently weights clusters by their size, unlike the Euler number; with the result that Γ(NW) is much less susceptible to noise which would manifest as falsely labeled NW voxels.

3.0 Materials and Methods

The complete experimental set-up and process is similar to that of Herring et al. [10] and only deviations from the previous study and the general process will be described here. Experiments were conducted with two 6.2 mm diameter Bentheimer sandstone cores of lengths of approximately 21 mm. Air was the NW fluid, and the W fluid was brine made of degassed millipore DI water doped with potassium iodide (KI), one part KI to six parts water by weight. The core was first vacuum-saturated with brine, and an x-ray tomographic scan was taken to characterize the original NW phase saturation (S_O) inside the core. Then brine was drained from the bottom of the core (as ambient air was passively pulled into the top of the core) at a flow rate of 0.2 ml/hr via a Harvard PHD2000 syringe pump (Harvard Apparatus, Holliston MA, United

States) to a preselected initial NW phase saturation (S_I) value (S_I values ranged from 42%-93%). The system was allowed to equilibrate until capillary pressure readings stabilized, and another tomographic scan was collected. Finally, brine was imbibed into the bottom of the core at one of three different flow rates (0.018 ml/hr, 1.8 ml/hr, or 54 ml/hr) as air was flushed out the top of the core, and a scan was acquired of the residual NW phase saturation (S_R). For three experiments, the core was dried under vacuum resulting in relatively high NW saturation (e.g. 94%-100% NW saturation), and the imbibition process was performed on the "dry" core. A pressure transducer (Validyne Engineering, Northridge CA, United States) with a range of 14.0 kPa was connected in parallel with the brine flow line to measure capillary pressure response.

Tomographic imaging was performed at the bending magnet beam-line at sector 13 (GSECARS) at the Advanced Photon Source at Argonne National Laboratory; specifications for the beamline have previously been reported [38-40]. Scans were performed at a monochromatic energy level of 33.269 keV, just above the K-shell photoelectric absorption edge of iodine (33.169 keV), resulting in x-ray attenuation by the KI-doped brine and thus allowing for separation of the W and NW fluids in the reconstructed images. Images were captured at 720 angles, with a voxel resolution of 5.8 µm.

After reconstruction, a cylindrical subsection of diameter 975 voxels and height 600 voxels (approximately 90 mm^3) was chosen which excludes the walls from the volumes (Figure 3a). This data size is larger than the determined REV for connectivity measures of 600 x 600 x 600 voxels, which is equivalent to a physical volume of 40 mm^3 (see supplemental materials online). A median filter was applied to smooth the images and reduce random noise (Figure 3b), and a histogram of the grayscale values present in each volume was calculated. The histogram minimum separating those grayscale values representing air and those representing sandstone grains or brine were determined for each volume (Figure 3d), and the threshold value was set equivalent to this minimum value resulting in the final binarized data volume (Figure 3c). Finally, a size exclusion filter was applied which removed air-labeled clusters less than 125 voxels; this volume corresponds to a spherical pore of radius 18 μm which is below the minimum pore size of Bentheimer (pore size distribution measured by Maloney et al. [41]). This process results in a binary image with only NW phase labeled. Avizo Fire ™ was then used to quantify NW saturation, cluster volumes, cluster numbers, and Euler numbers. The numerical methods utilized in Avizo Fire™ for quantification of Euler number values are detailed by Odgaard and Gundersen [35]; 26-neighborhood voxel connectivity is utilized for these calculations. All saturation values presented in the results are calculated from x-ray CMT images as opposed to the measured pumped by the syringe pump, as the accuracy of pumped volumes can suffer from dead volume and bubble effects.

4.0 Sensitivity of Connectivity Metrics to Image Quality

Because of their dependence on very small features, image-derived connectivity metrics may be sensitive to various image quality parameters, for example: noise levels, data resolution, the type of filters applied to the data, segmentation method, and segmentation threshold values. Additionally, in order to provide an accurate representation of the connectivity of the system, quantitative connectivity metrics must be calculated on an REV. An investigation into the sensitivity to these factors of both the normalized Euler value ($\hat{\chi}$) and Γ(NW) was conducted and is presented in the supplemental materials available online; for brevity, only the results are highlighted here. In order to examine the sensitivity of these parameters on a wider range of image-based data, the relatively high quality data (with respect to phase contrast, noise, and voxel resolution) presented in this study which was collected at the Advanced Photon Source at

Argonne National Lab at a resolution of 5.8 µm (denoted “APS” data) was compared to data presented in Herring et.al. [10] which was collected via a polychromatic bench-top x-ray CMT system at Oregon State University at a resolution of approximately 10 µm (denoted “OSU” data). Image parameters for both data sets are shown in Table A.1 in the supplementary materials.

Based on the analysis of the two data sets, we established the following conclusions regarding the significance of these image quality parameters on the calculation of $\hat{\chi}_{NW}$ or Γ(NW):

- Noise which manifests as small, isolated, falsely labeled NW voxels has no significant impact on Γ(NW); and no significant impact on $\hat{\chi}_{NW}$ as long as a minimum level of noise removal is applied. In the case of the high resolution APS data, noise reduction was achieved using a median filter on the grayscale image and by processing the segmented (binary) data to remove isolated NW clusters smaller than 52 voxels (equivalent to a sphere with a radius of 13 µm) was sufficient to provide consistent $\hat{\chi}_{NW}$ calculations.
- A representative elementary volume (REV) for the APS data is achieved at approximately 600 × 600 × 600 voxels (equivalent to a cube of 42.14 mm^3, or 3.48 mm per side) for both $\hat{\chi}_{NW}$ and Γ(NW) in Bentheimer sandstone. Use of an analytical volume smaller than the REV has a relatively small effect on the calculation of $\hat{\chi}_{NW}$, and a dramatic effect on the calculation of Γ(NW) .
- Image resolution has minimal impact on calculation of both $\hat{\chi}_{NW}$ and Γ(NW) for the range of resolution investigated (5.8 µm and 10 µm).
- Data processing schemes (i.e. filters and threshold detection method applied) have a significant effect on both $\hat{\chi}_{NW}$ and Γ(NW). The OSU data presented in Herring

et al. [10] was originally processed using ROCK3DMA, an Indicator Kriging segmentation algorithm [42]. Comparison of the original OSU Indicator Kriging results with the APS data (which was smoothed using a median filter, denoised, and segmented via simple grayscale histogram thresholding as described in Section 3) demonstrates disagreement in the $\hat{\chi}_{NW}$-saturation and Γ(NW)-saturation relationships and in absolute $\hat{\chi}_{NW}$ and Γ(NW) values. Reprocessing the grayscale OSU data by the same process as the APS data resolves this disagreement in the calculation of $\hat{\chi}_{NW}$, but Γ(NW) remains inconsistent between the data sets. This highlights that different data sets must processed and evaluated carefully to ensure accurate comparison.

- For data with unfavorable grayscale histograms due to the lack of distinctive peaks or poorly defined minima between the NW and solid/W phases, the choice of grayscale segmentation threshold has a minor effect on the calculation of Γ(NW), but a significant effect on the calculation of $\hat{\chi}_{NW}$. For these grayscale images (16 bit precision), changing the threshold by ±100 grayscale values results in approximately a ±20% shift in $\hat{\chi}_{NW}$ (Table A.2). For images with poorly defined histogram peaks, a consistent and objective threshold detection system is therefore necessary.

It is important to note that for the image quality parameters which are highly important to connectivity metric calculations (i.e. data processing procedure and threshold determination) the most significant impacts are imparted on the images with the most NW fluid present: the dry, or 100% NW fluid filled, scan of the porous medium. As indicated by Equation 6 and noted above, the determination of $\chi_{100\%NW}$ has a large impact on the analysis of the entire data set. Accurate acquisition, processing, and analysis of the dry scan of the medium is of great importance in ensuring the relevance and applicability of the overall data analysis.

As described in Section 3.0, for the relatively high quality experimental data of this study, all quantitative metrics are calculated on a data set larger than the required REV, and a median filter was utilized for noise removal and smoothing. The resulting histogram of measured grayscale values exhibited very well defined peaks (Figure 3d), allowing for accurate separation of NW and combined W/solid phases. Minimal post-segmentation noise removal (removal of isolated NW labeled clusters smaller than 125 voxels) was used. Based on the presented sensitivity analysis, we are confident that this procedure results in reliable quantitative values.

5.0 Results

5.1 Force Balance Analysis and Traditional Empirical Relationships

Traditionally, capillary trapping has been investigated by examining the various relationships between initial NW saturation (S_I), residual NW saturation (S_R), and imbibition capillary number (Ca); for example see Chatzis and Morrow [12], Chatzis et al. [16], Al Mansoori et al. [2], and Land [31]. Both capillary trapping efficiency (S_R/S_I) and total capillary trapping (S_R) are important parameters to CO_2 sequestration operations, and can be investigated as a function of S_I and imbibition Ca (Figure 4). The Bentheimer sandstone cores used in this study are relatively uniform and we expect a high level of consistency between experiments performed in different cores; thus, data presented in Figure 4 and subsequent figures include a combination of the results of both cores.

From the force balance analysis presented in Section 2.1, our Bentheimer-brine-air system is expected to be dominated by capillary and viscous forces; as is a supercritical CO_2-brine-sandstone system (given the range of supercritical CO_2 fluid properties attainable and assuming similar media to Bentheimer sandstone; red trapezoid in Figure 2). Thus, the residual state of both systems should depend on imbibition Ca. Bond number (Bo) values for the CO_2-brine-sandstone system are approximately an order of magnitude smaller than those for the Bentheimer-brine-air system (i.e. the CO_2-brine-sandstone system has less gravity force influence than the ambient condition experimental system, due to the relative similarity in CO_2 and brine densities as compared to the density difference of air and brine). However, neither system exists in a gravity dominated regime, so we expect that the ambient Bentheimer-brine-air system will produce results that are similar to a geologic CO2 sequestration operation.

As shown, the expected trends of decreased total NW capillary trapping (S_R) and decreased trapping efficiency (S_R/S_I) with increasing imbibition Ca are present (Figure 4a and 4b), as is the traditional Land's model description of increasing residual NW saturation with increasing initial NW saturation (Figure 4c). However, there is a large amount of scatter in the data which is not resolved by normalizing the residual saturation by the initial saturation, or by grouping the data by the imbibition Ca value; this discrepancy is investigated in the next section.

5.2 Inclusion of Connectivity

In order to understand the variability inherent in these results as described by the empirical models above, we consider how the connectivity of the NW phase impacts trapping results. First, though, we investigate how the connectivity characteristics of the normalized Euler characteristic ($\hat{\chi}$) and Γ(NW) manifest for NW fluid within porous media during the drainage process via the relationship between each connectivity metric and initial NW saturation (Figure 5).

Here the differences in these connectivity metrics are dramatically apparent. Γ(NW) approaches a value of unity at relatively low saturation, implying that the majority of the NW phase present is connected to the main cluster by at least one pore throat throughout the drainage process, with increasing probability that any isolated NW cluster will become connected to the main cluster as initial NW saturation increases. Above an initial NW saturation of approximately 80%, the variation in Γ(NW) is negligible; implying that at NW saturation at or above 80%, all NW phase is connected via at least one pore throat within the medium.

The $\hat{\chi}$ value provides a fundamentally different quantitative description of the NW fluid connectivity. At initial NW saturation greater than 50%, the number of NW clusters (β_0) roughly matches the number of connections within individual clusters (β_1), as indicated by $\hat{\chi}_{NW} \approx 0$. In direct comparison to Γ(NW), $\hat{\chi}$ shows the most dramatic growth at values greater than 80% NW saturation, i.e. long after the largest cluster has already formed as evaluated by Γ(NW). Γ(NW) values show that above 80%, almost all NW fluid is already connected and distinct individual fluid clusters are minimized, thus, the increase in $\hat{\chi}$ is due to the increase in redundant connections, β_1. Consideration of Γ(NW) and $\hat{\chi}_{NW}$ together demonstrates both the degree and manner of NW phase connectivity within the porous medium: for the post-drainage Bentheimer-air-brine system, the NW phase is largely connected via one large cluster; and as NW saturation increases, the NW phase invades additional pore throats *within* this single cluster.

This interpretation is further demonstrated by the approximately linear relationship between $\hat{\chi}$ and the equilibrium capillary pressure (the difference in pressure between the NW phase and the W phase) at the end of the drainage process (Figure 6). As capillary pressure increases, more (and smaller) pore throats are invaded, and $\hat{\chi}_{NW}$ increases.

A $\hat{\chi}$ value of zero provides an estimate of the percolation threshold; i.e. the NW saturation value at which NW phase fluid is connected throughout the porous medium, spanning the entirety of the domain [36, 37]. The relationship between initial $\hat{\chi}_{NW}$ and NW saturation demonstrated by the experimental data (Figure 5) shows that $\hat{\chi}_{NW} = 0$ at NW saturation of approximately 50% within Bentheimer sandstone. A computational approach for predicting pressure-saturation curves in media was described by Hazlet [43] and further by Hilpert and Miller [44] wherein morphological opening with a sphere of incrementally increasing radius is performed on a binary representation of a porous medium (i.e. the dry image of the medium), and saturation and pressure values are calculated by simulation at each opening step. A similar process was applied here, wherein the opening procedure was performed on binary volumes of dry Bentheimer sandstone using Avizo Fire™. After each opening step, isolated NW fluid clusters (<10,000 voxels or a sphere of radius 77.5 μm) resulting from the opening process which were not connected to the main fluid clusters were removed. $\hat{\chi}_{NW}$ and saturation values were calculated for each successive opening; the results of this analysis are compared with the experimental data (Figure 7). The morphological opening procedure conducted on the dry images resembles the $\hat{\chi}_{NW}$ values at initial saturation to within a reasonable approximation, demonstrates that $\hat{\chi}_{NW} = 0$ at NW phase saturation of 50% (providing additional evidence that the NW phase percolation threshold for Bentheimer sandstone is at a NW saturation of approximately 50%), and suggests that the $\hat{\chi}_{NW}$-saturation relationship for a given medium might be approximated from one high-quality (i.e. adequate resolution and low noise level) scan of a dry porous media rather than from multiple time-consuming experimental drainage observations.

Following Herring et al. [10], we investigate the impact of connectivity on capillary trapping efficiency (Figure 8); these data are classified by the imbibition process Ca as in Figure 4c. While both Γ(NW) and $\hat{\chi}_{NW}$ plots show a relationship between capillary trapping efficiency and connectivity, the relationship between normalized initial $\hat{\chi}_{NW}$ and trapping efficiency shows a strong linear correlation (Figure 8a), compared to Γ(NW) (Figure 8b) where the trend is non-linear due to insensitivity of Γ(NW) in the high NW saturation range. This suggests that while NW trapping is certainly related to the general connectivity of the NW phase, the capillary trapping/mobilization process is directly related to the NW topology as described by the Euler characteristic. An increase in the number of redundant pore throats (β_1) which connect NW fluid *within* the fluid clusters, that is, a higher initial $\hat{\chi}_{NW}$ value, is equivalent to a higher number of potential pathways through which NW fluid can be mobilized, and results in decreased trapping efficiency. Note also that the high and intermediate imbibition Ca data show a relatively strong dependence on initial $\hat{\chi}_{NW}$ (slope of approximately -0.3 for both, R^2= 0.92 and 0.98 respectively) whereas low imbibition Ca experimental data exhibits much lower dependence (slope of -0.12, R^2=0.37). This suggests that fluid topology as described by $\hat{\chi}$ plays a strong role in fluid mobilization during flow dominated by viscous forces, but has reduced impact during capillary dominated flow.

The relationship between residual trapping (S_R) and initial NW $\hat{\chi}$ illustrates these results from a slightly different perspective (Figure 9); here a parabolic trend is evident for each imbibition Ca category. Maximum residual NW saturation, i.e. the maximum trapping capacity of the medium, is reached at a moderate initial $\hat{\chi}_{NW}$ value ($\hat{\chi}_{NW} \approx 0.4$) for both high ($10^{-5.1}$) and intermediate ($10^{-6.6}$) Ca imbibition values, and trapping capacity is unaffected by the initial NW $\hat{\chi}$ for low ($10^{-8.6}$) Ca imbibition.

6.0 Conclusion and Application to CO_2 sequestration

This work has presented the results of x-ray CMT quantified experiments of drainage and imbibition with a wetting (W) phase of 1:6 by weight KI brine and nonwetting (NW) phase of air within Bentheimer sandstone. We have determined, based on a pore-scale force analysis, that capillary and viscous forces will dominate the system rather than gravity forces. We have shown experimentally that the residual state of the system is indeed sensitive to changes in capillary number (Ca), which describes the relative importance of capillary and viscous forces in a multiphase system. We have also investigated two different quantitative connectivity metrics and shown that NW phase trapping and mobilization is well described by the normalized Euler number of the NW phase ($\hat{\chi}_{NW}$) after drainage: a more highly connected NW phase is connected by a high number of redundant pore throats, which allows for more NW phase to be mobilized, thus resulting in less NW phase capillary trapping. The dependence of capillary trapping on NW phase $\hat{\chi}$ is more pronounced for systems in a viscosity dominated regime; for capillary-dominated systems (low Ca), the NW phase connectivity has less impact on the final NW trapping. This is consistent with standard understanding of displacement mechanisms: at sufficiently low flow rates the small pore throats that provide improved NW connectivity become water-filled by the process of "snap-off" early in the imbibition process; at higher flow rates snap-off is suppressed (e.g. [18]), so the connections through small pore throats remain open longer and therefore have a greater effect on the residual saturation. We note here that additional theoretical analysis is needed to completely describe the physics underlying the correlations between connectivity and capillary trapping.

Sedimentary reservoirs are proposed to be optimal storage sites for CO_2 sequestration due to the stratigraphy of porous, permeable sandstone and carbonate layers (which act as storage layers) and relatively impermeable silt and shale stone layers (which act as caprocks) [45, 46]. Given the range of supercritical CO_2 fluid properties attainable in a sequestration operation, and in similar media to Bentheimer sandstone, the supercritical CO_2-brine-sandstone system will be dominated by capillary and viscous forces at the pore scale (Figure 2), and fall in the same general area of the force balance plot as the air-brine-Bentheimer experiments presented here. Thus, we expect that pore scale capillary trapping and mobilization of supercritical CO_2 during sequestration to behave similarly to the air-brine-Bentheimer system examined here. Indeed, Herring, et al. [11] found that micromodel studies of ambient-state NW phase invasion were able to accurately predict the flow pattern of supercritical CO_2 during drainage in Bentheimer sandstone by consideration and proper dimensional analysis of fluid properties.

Comparison of Figure 4c with a typical Land's model curve (e.g. Al Mansoori et al. [2]) demonstrates that the plateau in NW S_R values that is apparent above approximately 50% initial NW saturation is due to the percolation threshold being exceeded during the drainage process. Further, the data presented here shows that for a system at an initial NW saturation approaching 100% (and thus, maximum NW connectivity, $\hat{\chi}_{NW} = 1.0$), capillary trapping is further suppressed and NW S_R actually decreases. This has important implications for CO_2 sequestration operations, where high CO_2 saturations may exist near the injection site, and where dry-out conditions may occur [47]. Dry-out occurs when CO_2 which is in chemical non-equilibrium with brine is injected into the subsurface, causing the resident brine to dissolve into the CO_2 phase and creating subsurface areas where NW phase saturation approaches 100%; if brine salinity is sufficiently high, dry-out may cause salt precipitation leading to reduced permeability [47].

In the example of a geologic CO_2 sequestration operation, Figures 8a and 9 imply that two distinct methodologies could be used to maximize capillary trapping, depending on the desired result. To maximize capillary trapping *efficiency* (S_R/S_I), and ensure that the largest fraction of injected CO_2 is immobilized in the pore space of the reservoir, the CO_2 injection should be engineered to result in low initial $\hat{\chi}_{NW}$ (e.g. initial $\hat{\chi}_{NW} \leq 0.1$, or $S_I \leq 0.75$). This would provide for additional storage security beyond relying on a structural/stratigraphic trapping layer. In contrast, in order to utilize the maximum trapping capacity of the pore space, CO_2 injection should be engineered to result in moderate initial $\hat{\chi}_{NW}$ (e.g. $\hat{\chi}_{NW} = 0.4$, or $S_I \approx 0.85$). For either goal, dry-out conditions should be avoided. Manipulation of initial $\hat{\chi}_{NW}$ could potentially be accomplished via use of a water-alternating-gas scheme (as proposed by Spiteri et al. [48]), which may have significant water use impacts; or via manipulation of injection patterns to inject to intermediate saturations. For example, one suggestion would be to have a shorter vertical injection interval in the injection well: injection only into the lower portions of the aquifer would allow for vertical migration and might prevent the CO_2 plume from approaching high saturation levels at the injection point. Alternatively, the subsequent imbibition process should be carried out at very low Ca regime, where NW topology does not impact residual saturation or capillary trapping efficiency. Manipulation of far-from-wellbore saturation can be achieved for well-characterized aquifers by designing the injection program in conjunction with large-scale simulation.

Acknowledgements

This material is based upon work supported by the U.S. Department of Energy, Basic Energy Sciences, Geosciences Program under award number DE-FG02-11ER16277, and also through the LANL/LDRD Program (#20100025DR). This research used resources of the Advanced Photon Source which is a DOE Office of Science User Facility. We acknowledge the support of GeoSoilEnviroCARS (Sector 13), which is supported by the National Science Foundation - Earth

Sciences (EAR-1128799), and the Department of Energy, Geosciences (DE-FG02-94ER14466). We are grateful to the GSECARS staff for technical support during beam-time, in particular Dr. Mark Rivers. Linnéa Andersson wishes to acknowledge funding from the Swedish Science Council. Steffen Schlüter is grateful to the Alexander-von-Humboldt-Foundation for granting a Feodor-Lynen-Scholarship. The research of Adrian Sheppard is supported by an Australian Research Council Future Fellowship (FT100100470).

References

[1] Juanes R, EJ Spiteri, FM Orr, Jr., MJ Blunt. Impact of relative permeability hysteresis on geological co2 storage. Water Resour Res. 42 (2006) W12418, doi: 10.1029/2005wr004806.

[2] Al Mansoori SK, E Itsekiri, S Iglauer, CH Pentland, B Bijeljic, MJ Blunt. Measurements of non-wetting phase trapping applied to carbon dioxide storage. International Journal of Greenhouse Gas Control. 4 (2010) 283-8, doi: http://dx.doi.org/10.1016/j.ijggc.2009.09.013.

[3] Akbarabadi M, M Piri. Relative permeability hysteresis and capillary trapping characteristics of supercritical co2/brine systems: An experimental study at reservoir conditions. Advances in Water Resources. 52 (2013) 190-206.

[4] Andrew M, B Bijeljic, MJ Blunt. Pore-scale imaging of geological carbon dioxide storage under in situ conditions. Geophysical Research Letters. 40 (2013) 3915-8, doi: 10.1002/grl.50771.

[5] IPCC. Ipcc special report on carbon dioxide capture and storage, 2005.

[6] Bachu S, DB Bennion. Interfacial tension between co2, freshwater, and brine in the range of pressure from (2 to 27) mpa, temperature from (20 to 125) °c, and water salinity from (0 to 334 000) mg·l−1. Journal of Chemical & Engineering Data. 54 (2008) 765-75, doi: 10.1021/je800529x.

[7] Bachu S, B Bennion. Effects of in-situ conditions on relative permeability characteristics of co_2-brine systems. Environmental Geology. 54 (2008) 1707-22, doi: 10.1007/s00254-007-0946-9.

[8] Bachu S, D Brant Bennion. Dependence of co2 -brine interfacial tension on aquifer pressure, temperature and water salinity. Energy Procedia. 1 (2009) 3157-64, doi: 10.1016/j.egypro.2009.02.098.

[9] Akbarabadi M, M Piri. Relative permeability hysteresis and capillary trapping characteristics of supercritical co< sub> 2</sub>/brine systems: An experimental study at reservoir conditions. Advances in Water Resources. (2012).

[10] Herring AL, EJ Harper, L Andersson, A Sheppard, BK Bay, D Wildenschild. Effect of fluid topology on residual nonwetting phase trapping: Implications for geologic co2 sequestration. Advances in Water Resources. 62 (2013) 47-58.

[11] Herring AL, L. Andersson, D.L. Newell, J.W. Carey, D. Wildenschild. Pore-scale observations of supercritical co2 drainage in bentheimer sandstone by synchrotron x-ray imaging. International Journal of Greenhouse Gas Control. In Press (2014).

[12] Chatzis I, NR Morrow. Correlation of capillary number relationships for sandstone. Journal Name: SPEJ, Soc Pet Eng J; (United States); Journal Volume: 24:5. (1984) Medium: X; Size: Pages: 555-62.

[13] Jamaloei BY, K Asghari, R Kharrat. The investigation of suitability of different capillary number definitions for flow behavior characterization of surfactant-based chemical flooding in heavy oil reservoirs. Journal of Petroleum Science and Engineering. 90–91 (2012) 48-55, doi: 10.1016/j.petrol.2012.04.020.

[14] Cense AW, S Berg. The viscous-capillary paradox in 2-phase flow in porous media. International Symposium of the Society of Core Analysts. Shell International Exploration & Production, Noordwijk, The Netherlands, 2009.

[15] Morrow NR, I Chatzis, JT Taber. Entrapment and mobilization of residual oil in bead packs. Journal Name: SPE (Society of Petroleum Engineers) Reserv Eng; (United States); Journal Volume: 3:3. (1988) Medium: X; Size: Pages: 927-34.
[16] Chatzis I, MS Kuntamukkula, NR Morrow. Effect of capillary number on the microstructure of residual oil in strongly water-wet sandstones. Journal Name: SPE (Society of Petroleum Engineers) Reserv Eng; (United States); Journal Volume: 3:3. (1988) Medium: X; Size: Pages: 902-12.
[17] Suekane T, N Zhou, T Hosokawa, T Matsumoto. Direct observation of trapped gas bubbles by capillarity in sandy porous media. Transport in Porous Media. 82 (2010) 111-22, doi: 10.1007/s11242-009-9439-5.
[18] Hughes RG, MJ Blunt. Pore scale modeling of rate effects in imbibition. Transport in Porous Media. 40 (2000) 295-322, doi: 10.1023/a:1006629019153.
[19] Nguyen VH, AP Sheppard, MA Knackstedt, W Val Pinczewski. The effect of displacement rate on imbibition relative permeability and residual saturation. Journal of Petroleum Science and Engineering. 52 (2006) 54-70, doi: 10.1016/j.petrol.2006.03.020.
[20] Ding M, A Kantzas. Capillary number correlations for gas-liquid systems. Society of Petroleum Engineers, Calgary, CANADA, 2007.
[21] Mayer AS, CT Miller. An experimental investigation of pore-scale distributions of nonaqueous phase liquids at residual saturation. Transp Porous Med. 10 (1993) 57-80.
[22] Harper EJH, A.L.; Armstrong, R.T.; Lunati, I.; Bay, B.K.; Wildenschild, D. On the optimization of capillary trapping during geologic co2 sequestration. In prep (2014).
[23] Geistlinger, H., S. Mohammadian, S. Schlueter, and H.-J. Vogel (2014), Quantification of capillary trapping of gas clusters using X-ray microtomography, Water Resour. Res., 50, 4514–4529, doi:10.1002/ 2013WR014657.
[24] Mohammadian S, H Geistlinger, H-J Vogel. Quantification of gas-phase trapping within the capillary fringe using computed microtomography. gsvadzone. 0 (2014) -, doi: 10.2136/vzj2014.06.0063.
[25] Polak S, Y Cinar, T Holt, O Torsæter. An experimental investigation of the balance between capillary, viscous, and gravitational forces during co2 injection into saline aquifers. Energy Procedia. 4 (2011) 4395-402, doi: 10.1016/j.egypro.2011.02.392.
[26] Armstrong RT, A Georgiadis, H Ott, D Klemin, S Berg. Critical capillary number: Desaturation studied with fast x-ray computed microtomography. Geophysical Research Letters. 41 (2014) 2013GL058075, doi: 10.1002/2013gl058075.
[27] Andrew M, B Bijeljic, MJ Blunt. Pore-by-pore capillary pressure measurements using x-ray microtomography at reservoir conditions: Curvature, snap-off, and remobilization of residual co2. Water Resources Research. 50 (2014) 8760-74, doi: 10.1002/2014wr015970.
[28] Mayer AS, CT Miller. The influence of porous medium characteristics and measurement scale on pore-scale distributions of residual nonaqueous-phase liquids. Journal of Contaminant Hydrology. 11 (1992) 189-213.
[29] Gittins P, S Iglauer, CH Pentland, S Al-Mansoori, S Al-Sayari, B Bijeljic, et al. Nonwetting phase residual saturation in sand packs. Journal of Porous Media. 13 (2010) 591-9.
[30] Morrow NR. Physics and thermodynamics of capillary action in porous media. Industrial & Engineering Chemistry. 62 (1970) 32-56, doi: 10.1021/ie50726a006.
[31] Land C. Calculation of imbibition relative permeability for two-and three-phase flow from rock properties. Old SPE Journal. 8 (1968) 149-56.

[32] Wardlaw NC, L Yu. Fluid topology, pore size and aspect ratio during imbibition. Transp Porous Med. 3 (1988) 17-34.
[33] Renard P, D Allard. Connectivity metrics for subsurface flow and transport. Advances in Water Resources. 51 (2013) 168-96.
[34] Pathak P, HT Davis, LE Scriven. Dependence of residual nonwetting liquid on pore topology. Society of Petroleum Engineers1982.
[35] Odgaard A, HJG Gundersen. Quantification of connectivity in cancellous bone, with special emphasis on 3-d reconstructions. Bone. 14 (1993) 173-82, doi: http://dx.doi.org/10.1016/8756-3282(93)90245-6.
[36] Vogel HJ. Topological characterization of porous media. Morphology of Condensed Matter. (2002) 75-92.
[37] Mecke K, H Wagner. Euler characteristic and related measures for random geometric sets. Journal of statistical physics. 64 (1991) 843-50.
[38] Wildenschild D, CMP Vaz, ML Rivers, D Rikard, BSB Christensen. Using x-ray computed tomography in hydrology: Systems, resolutions, and limitations. Journal of Hydrology. 267 (2002) 285-97, doi: 10.1016/s0022-1694(02)00157-9.
[39] Wildenschild D, J Hopmans, M Rivers, A Kent. Quantitative analysis of flow processes in a sand using synchrotron-based x-ray microtomography. Vadose Zone Journal. 4 (2005) 112-26.
[40] Rivers ML, SR Sutton, PJ Eng. Geoscience applications of x-ray computed microtomography. SPIE's International Symposium on Optical Science, Engineering, and Instrumentation. International Society for Optics and Photonics1999. pp. 78-86.
[41] Maloney DR, MM Honarpour, AD Brinkmeyer. The effects of rock characteristics on relative permeability. 1990. pp. Medium: X; Size: Pages: (29 p).
[42] Oh W, B Lindquist. Image thresholding by indicator kriging. Pattern Analysis and Machine Intelligence, IEEE Transactions on. 21 (1999) 590-602.
[43] Hazlett R. Simulation of capillary-dominated displacements in microtomographic images of reservoir rocks. Transp Porous Med. 20 (1995) 21-35.
[44] Hilpert M, CT Miller. Pore-morphology-based simulation of drainage in totally wetting porous media. Advances in Water Resources. 24 (2001) 243-55, doi: 10.1016/s0309-1708(00)00056-7.
[45] Bachu S. Screening and ranking of sedimentary basins for sequestration of co2 in geological media in response to climate change. Environmental Geology. 44 (2003) 277-89, doi: 10.1007/s00254-003-0762-9.
[46] Gunter WD, S Bachu, S Benson. The role of hydrogeological and geochemical trapping in sedimentary basins for secure geological storage of carbon dioxide. Geological Society, London, Special Publications. 233 (2004) 129-45, doi: 10.1144/gsl.sp.2004.233.01.09.
[47] Pruess K, N Müller. Formation dry-out from co2 injection into saline aquifers: 1. Effects of solids precipitation and their mitigation. Water Resources Research. 45 (2009) W03402, doi: 10.1029/2008wr007101.
[48] Spiteri E, R Juanes, MJ Blunt, FM Orr. Relative-permeability hysteresis: Trapping models and application to geological co2 sequestration. SPE Annual Technical Conference and Exhibition. Society of Petroleum Engineers2005.

Figures

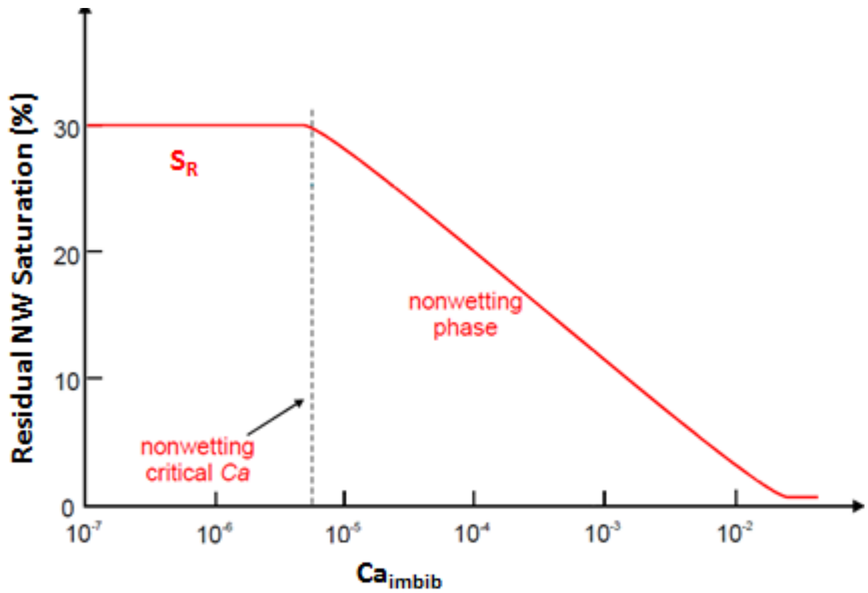

Figure 1. Capillary trapped residual nonwetting (NW) phase saturation (S_R) as a function of imbibition capillary number (Ca_{imbib}), modified from Cense and Berg [1].

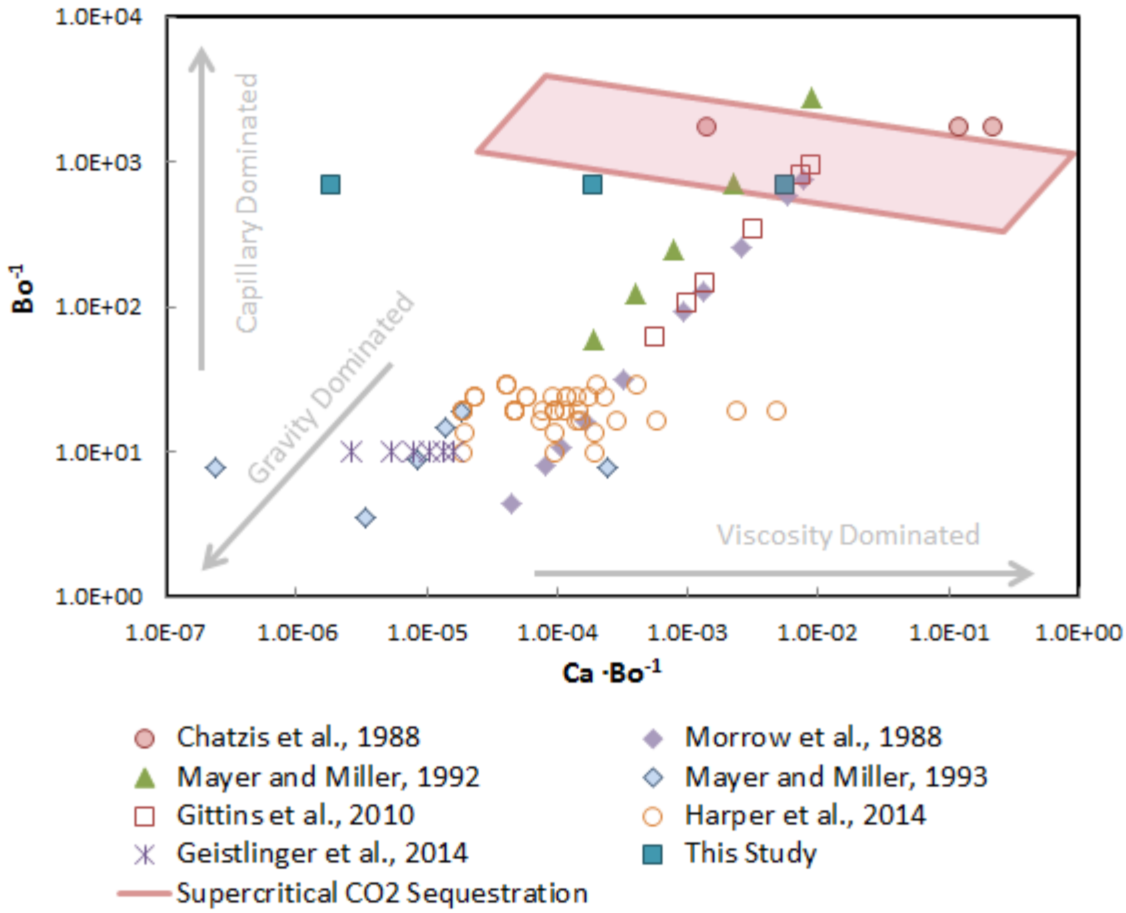

Figure 2. The locations of imbibition processes of previous works, the experiments of this study, and an approximate range for supercritical CO_2 sequestration (red rhomboid) within the pore scale force balance. Inverse Bond number (Bo^{-1}) describes the balance between capillary and gravity forces, and the product of capillary number (Ca) and Bo^{-1} describes the balance between viscosity and gravity forces.

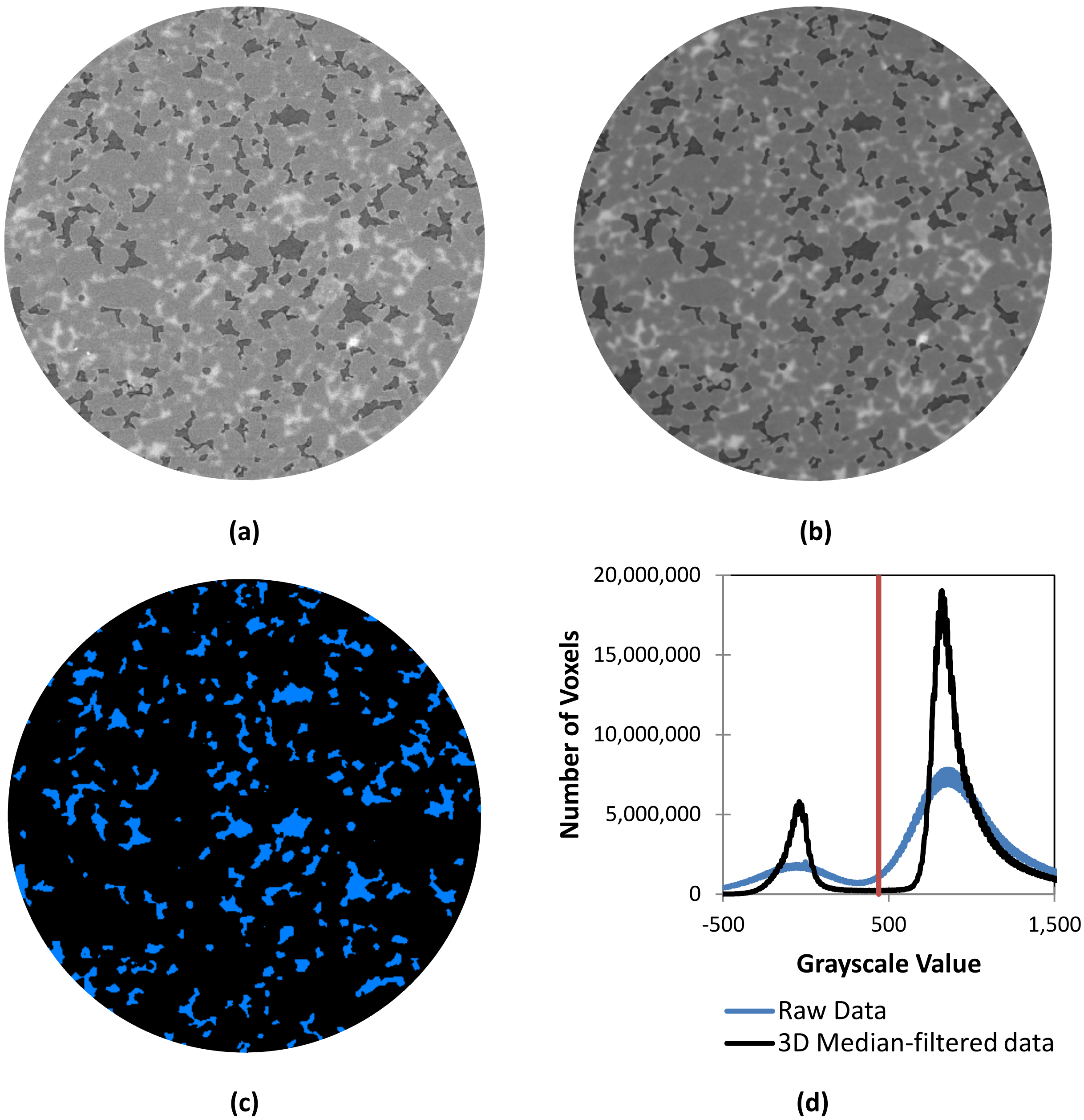

Figure 3. A cross-sectional slice of (a) raw data, (b) data after application of a three-dimensional (3D) median filter, and (c) binary data with the nonwetting (NW) phase identified. The grayscale histogram of the data volume for both raw and 3D median-filtered data is shown in (d) with the grayscale threshold value indicated.

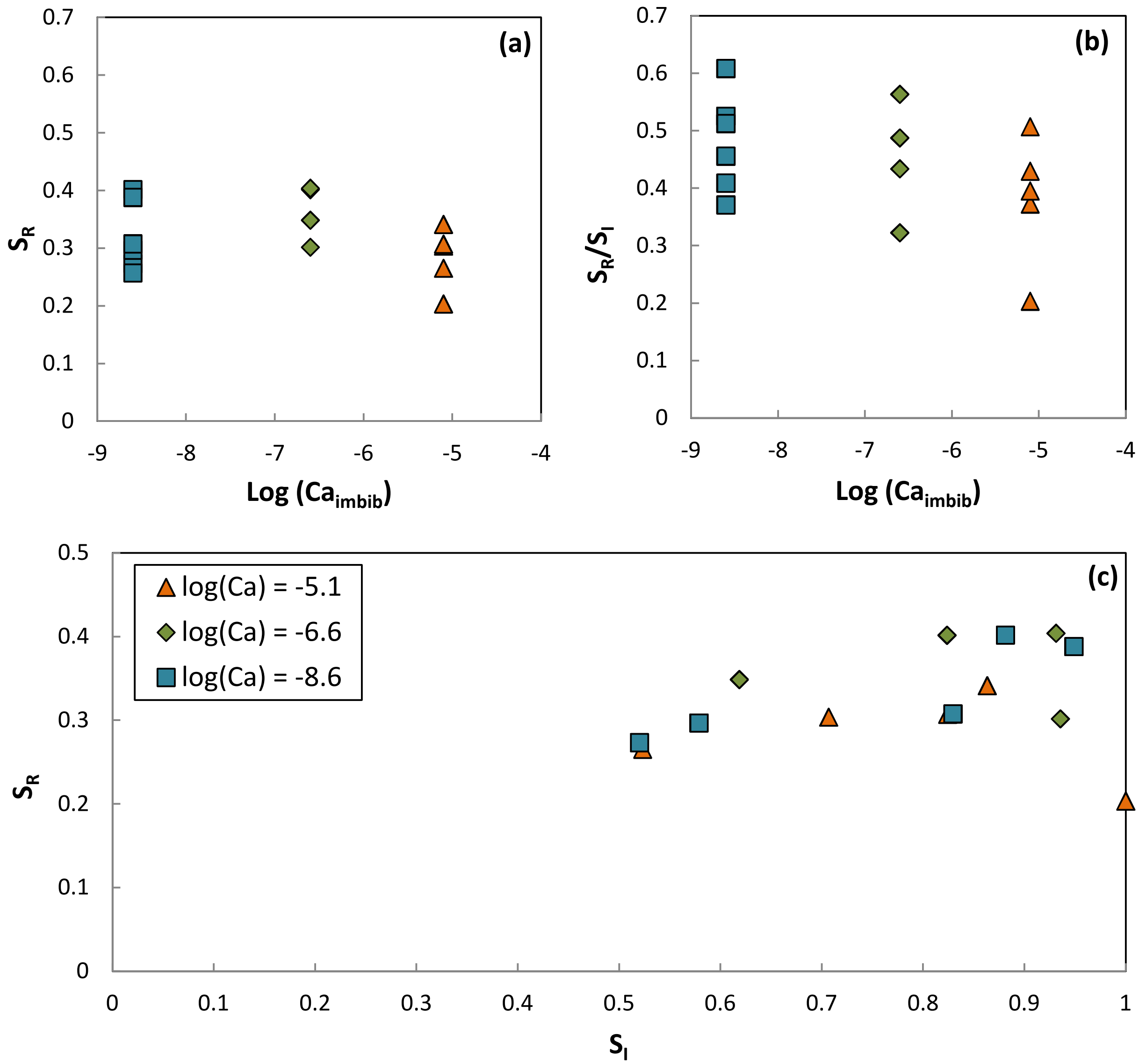

Figure 4. Results of drainage-imbibition experiments presented as (a) residual saturation (S_R) as a function of imbibition capillary number (Ca_{imbib}); (b) trapping efficiency, calculated as residual saturation normalized by initial saturation (S_I), as a function of imbibition Ca; and (c) residual saturation as a function of initial saturation (i.e. the traditional Land's model formulation [3, 31]) where experiments are classified by the imbibition Ca class as noted in the legend.

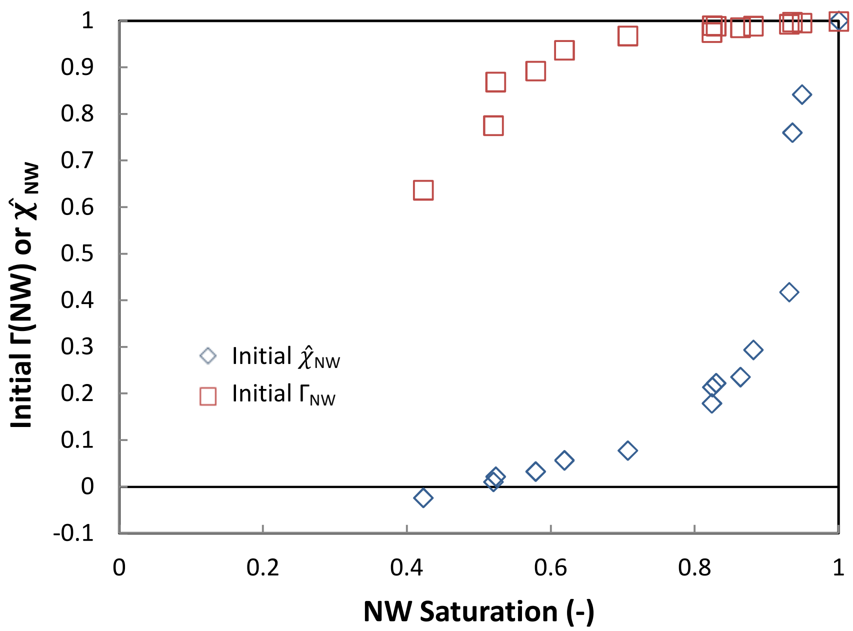

Figure 5. Connectivity of nonwetting (NW) phase at the initial system state as measured by Γ(NW) and initial normalized Euler value ($\hat{\chi}_{NW}$) as a function of NW saturation within Bentheimer sandstone.

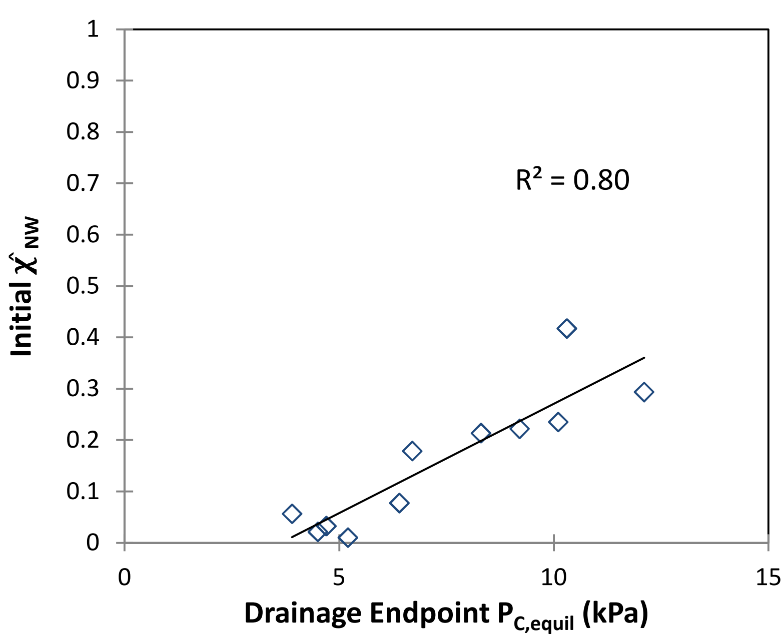

Figure 6. Initial nonwetting (NW) normalized Euler value ($\hat{\chi}_{NW}$) versus capillary pressure (P_C) after an equilibration period at the end of the drainage process within Bentheimer sandstone.

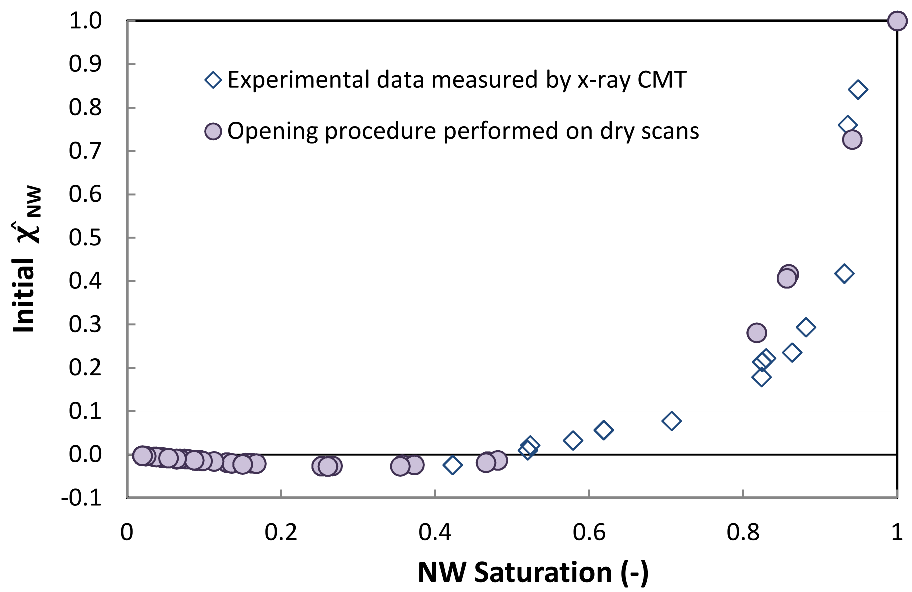

Figure 7. Initial nonwetting (NW) normalized Euler value ($\hat{\chi}_{NW}$) as a function of NW saturation within Bentheimer sandstone for experimental x-ray microtomography (x-ray CMT) data and for a computational morphological opening process performed on binary data of the dry sandstone.

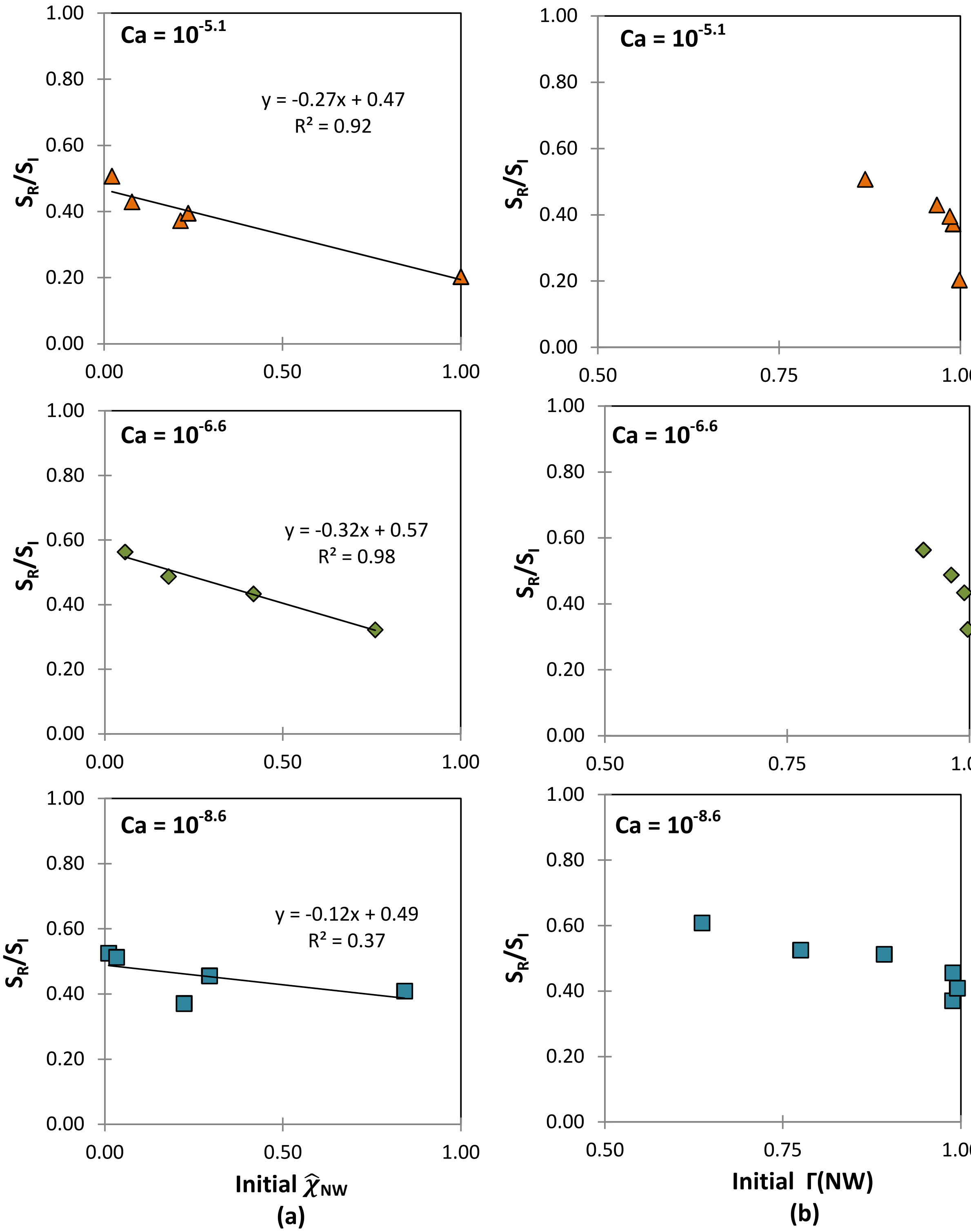

Figure 8. Capillary trapping efficiency of nonwetting (NW) phase, as described by residual NW saturation (S_R) normalized by initial NW saturation (S_I), as a function of (a) normalized initial NW Euler value (initial $\hat{\chi}_{NW}$) and (b) initial Γ(NW). Data are classified by the experimental imbibition capillary number (Ca).

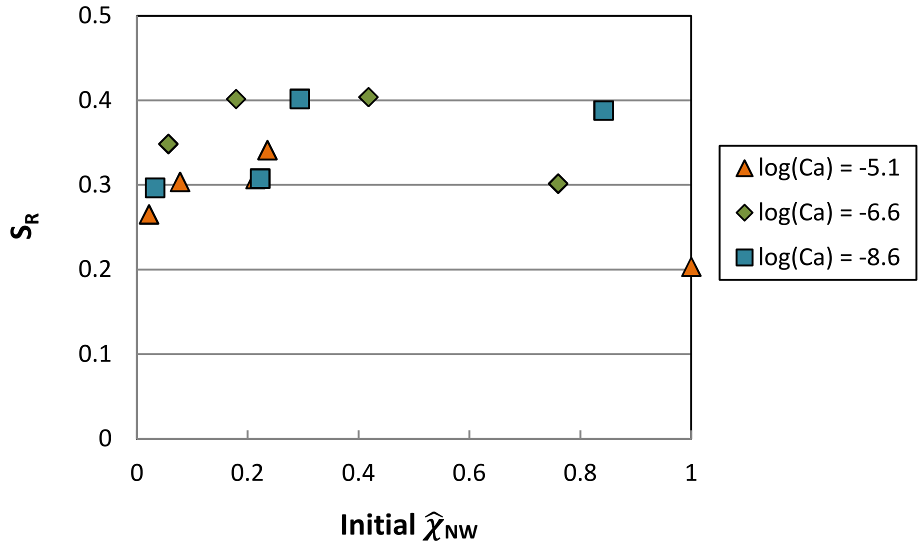

Figure 9. Residual capillary trapped nonwetting (NW) phase (S_R) as a function of normalized initial NW Euler value (Initial $\hat{\chi}_{NW}$). Data are classified by the experimental imbibition capillary number (Ca).